Materials Transactions, Vol. 60, No. 9 (2019) pp. 1792 to 1798
Special Issue on Latest Research and Development of Structural and Functional Titanium-Based Materials

Mechanical Properties of Additively Manufactured Porous Titanium with Sub-Millimetre Structural Units

Masato Ueda[1,*], Masahiko Ikeda[1], Shigeo Mori[2], Kenji Doi[2], Hisashi Kitagaki[2] and Shuntaro Terauchi[2]

[1]*Department of Chemistry and Materials Engineering, Faculty of Chemistry, Materials and Bioengineering, Kansai University, Suita 564-8680, Japan*
[2]*Osaka Yakin Kogyo Co., Ltd., Osaka 533-0005, Japan*

The mechanical properties of metallic materials can be controlled by both alloy design and the construction of an appropriate structure. Porous materials are a promising candidate for bone-related devices because they have a low Young's modulus and allow bone ingrowth. Recently, great advancements have been made in additive manufacturing technology, also known as three-dimensional printing. This technology enables the arbitrary and independent control of the Young's modulus, strength of the material, the shape and volume fraction of the pores. Porous titanium samples composed of rhombicuboctahedron-derived units with sub-millimetre dimensions were fabricated by laser additive manufacturing, and the dependence of their mechanical properties on the structural parameters was investigated. Porous Ti samples with five different sets of dimensions were accurately fabricated as designed. The solid Ti parts of the samples were confirmed to contain no remarkable solidification voids by Archimedes' principle. The porosity can be easily controlled in the present structural design; the measured and designed porosities showed a good linear relationship, although the measured porosity was slightly larger than the designed porosity. The gradient of stress-strain curve in elastic region can be also arbitrarily controlled in porous Ti samples with the present structure; it increased as the minimum cross-sectional area ratio in the plane perpendicular to the loading axis increased. This means that Young's modulus can be arbitrarily controlled by the present structural control. However, it should be noted that the local mechanical properties such as Young's modulus of the fabricated samples are not uniform in the overall structures; to improve this, the effect of the structure on the retention and flow of heat must be considered.
[doi:10.2320/matertrans.ME201916]

(Received February 6, 2019; Accepted May 7, 2019; Published June 14, 2019)

Keywords: *titanium, porous devices, 3D printing, Young's modulus, structural design*

1. Introduction

Titanium and its alloys have been used successfully in orthopaedic and dental applications for many years because of their excellent mechanical properties, biocompatibility, and reliability. In orthopaedic surgery, however, metallic materials often cause stress shielding due to mismatch of Young's modulus between the implants and the surrounding bone. For example, the Young's moduli of pure Ti and cortical bone are 110 and 10–30 GPa, respectively. As a result of this mismatch, the bone around such metallic implants is insufficiently loaded, thus causing bone atrophy.[1)] Eventually the implants loosen clinical performance.

The mechanical properties of metallic materials can be controlled by both metallurgical methods[2–4)] and structural design.[5–8)] In the latter, introduction of pores can effectively reduce Young's modulus. The porous structure can not only imitate structure and mechanical properties of living bone, but also facilitate bone ingrowth into the porous structure. Therefore such porous implants has long been sought as the ideal bone substitute.[9)] For example, porous Ti compacts have been fabricated in the porosity range of 5–37 vol% by controlling by powder size and sintering conditions.[10)] In the same study, it was shown that the Young's modulus and the proof and bend stresses are inversely proportional to the porosity; the fabricated compacts with a porosity of approximately 30 vol% showed mechanical properties equivalent to those of human cortical bone.

In another previous study, porous Ti was fabricated by the space holder method,[11)] which is a very simple method of preparing porous devices with random pores. Porous Ti with a random pores and a porosity of 60% were implanted in the tibial metaphyses of rats. Then, histological analysis was carried out after Villanueva–Goldner staining for newly formed bone around the implanted porous Ti. An ingrowth of mineralised bone was confirmed to have formed from the cortical bone growing into the pores. In addition, osteoid also penetrated into the pores of the device where it came into contact with cancellous bone or bone marrow. Such porous devices appear to be adequate as bone substitutes. Thus, it is desirable that all pores are connected from the viewpoint of bone ingrowth. In random pores, all pores are connected when the porosity is 60% or more. However, the space holder method implemented in this previous study has limitations in terms of the control of mechanical properties in the devices to be integrated with bones because the Young's modulus and strength of the device and the shape and volume fraction of the pores cannot be controlled independently.

Living bone is classified into dense cortical bone and spongy cancellous bone. Both are heterogeneous natural composite materials composed of biological apatite and collagen fibres. In line with their structures, cortical bone and cancellous bone provide mainly load-supporting and a calcium metabolism functions, respectively. Bone is known to be characterised by anisotropic mechanical properties.[12,13)] The preferential alignment of biological apatite in the calcified tissue of bone varies depending on the shape and stress conditions in vivo; the *c*-axes of biological apatite and collagen fibres in long bones are preferentially aligned in the longitudinal direction. Thus, it is extremely important to control the anisotropy of implantable parts in the fabrication of bone-related devices such as replacement joints and partial replacements. However, the target anisotropy cannot be reproduced in porous materials with random pores.

*Corresponding author, E-mail: m-ueda@kansai-u.ac.jp

Recently, great advancements have been made in additive manufacturing (AM) technology, also commonly known as three-dimensional (3D) printing. Powder bed fusion is a common technology used in 3D printing, particularly when applied to metallic materials. This layer-by-layer fabrication technique is well suited to the design and production of tailor-made metallic products with complex shapes, including porous materials, especially for medical applications such as artificial bone and replacement joints.[14–17] Actually, additive manufactured implants have been successfully used in clinical applications in several implant sites such as the skull, cheekbone, and mandible.[18,19] By this technique, furthermore, porosity and mechanical property can be controlled independently. This is an important advantage in medical device fabrications. For example, when a porous device is used as a partial replacement for bone, penetration of bone into the pores occurs. As a result, Young's modulus of the corresponding device must increase according to the law of mixtures. Ideally, it should be designed so that the mechanical property of the porous device-living bone composite will be similar to that of surrounding living bone after complete healing. Such devices can be easily realised by this technology.

In the future, such applications will undoubtedly expand rapidly; however, it will necessitate to develop AM techniques for modelling fine structures with sub-millimetre scale in order to give further advanced functions.

The aim of this study was to fabricate a small porous structure composed of units with sub-millimetre dimensions from pure Ti powder by AM. The target device has a simple structure that makes it easy to fabricate using conventional AM techniques. Additionally, the mechanical properties of porous Ti were investigated.

2. Experimental Procedures

2.1 Design and fabrication of porous structure

The computer-aided design (CAD) of the porous structure was conducted using Shade 3D professional 15.0.1 (Shade 3D Co., Ltd.) in this study.

In general, the structure having orthogonal planes has a limitation in modelling directions. It is also known that the microstructure is strongly influenced by the modelling direction; it must affect the mechanical properties. In this study, rhombicuboctahedron-derived units were used to design the structure, as shown in Fig. 1, and the entire porous structure consisted of 216 units ($6 \times 6 \times 6$ in the width, in-plane depth, and height directions). This structure can be easily manufactured in any direction because it does not have orthogonal planes. The structural characteristics of the design, such as its porosity and anisotropy, can be easily controlled by changing the parameters at the points of connection of the units in the horizontal and the vertical directions. However, there is concern that the heat flux might increase at the connection portions of unit structures compared with other portions.

In the present study, five types of porous Ti structures and one dense structure were designed. The dimensions of the individual units and the entire structures are listed in Table 1. The apparent shape of the overall porous Ti structure is a rectangular parallelepiped. The upper and lower faces of the units at the connection interfaces are squares. In this porous structure, the height direction is the load axis in the compressive test described below. The connection faces of each unit, i.e. the planes of the smallest horizontal cross-sectional area, seem to play a dominant role in determining the mechanical properties of the structure. Thus, the minimum cross-sectional area ratio in the horizontal plane of the different porous Ti structures were calculated and are listed in Table 1. In addition, the filling fraction of Ti is also given in Table 1. A wide range of porosities can be created with this structural design.

A pure Ti powder (ASTM grade 2, average particle size $< 23\,\mu m$) was prepared by gas atomisation. Samples were fabricated with the EOSINT M 270 laser AM machine (EOS, Germany), which has a 200 W fibre laser with high

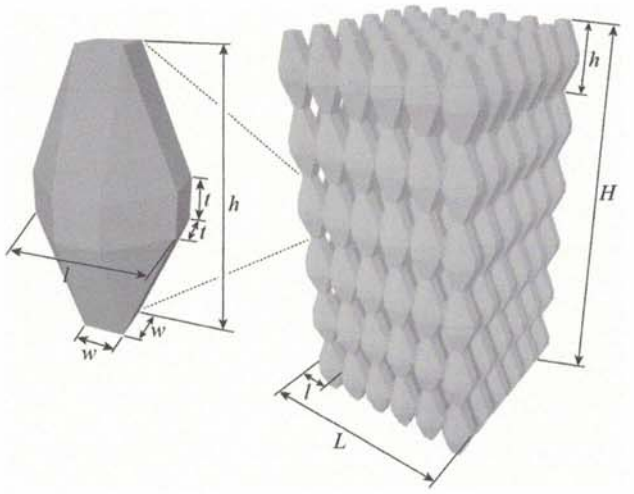

Fig. 1 Design of porous structure consisting of rhombicuboctahedron-derived units.

Table 1 Dimensions of the units and entire structures of the designed porous Ti samples, minimum cross-sectional area ratio in the horizontal plane, and calculated filling fraction of Ti.

w/l	Minimum cross sectional area ratio	Filling fraction	Dimensions of unit structure (mm)				Sample size (mm)	
			w	l	h	t	L	H
0.30	0.09	0.44	0.30	1.00	2.00	0.30	6.00	12.00
0.35	0.12	0.47	0.35					
0.60	0.36	0.65	0.60					
0.80	0.64	0.80	0.80					
0.95	0.90	0.92	0.95					
Dense	1.00	1.00	-					

Table 2 Process conditions for the laser additive manufacturing of the porous Ti samples.

Laser Power	120 W
Scan speed	200 μms^{-1}
Scan pitch	180 μm
Lamination pitch	30 μm
Atmosphere	Ar

beam quality good power stability. The process parameters used to fabricate the samples are given in Table 2, which are empirically optimised for the Ti powder. The porous samples were protected with the holders and then the base parts were carefully removed by a wet polishing.

2.2 Density

Two types of densities were measured for the additively manufactured porous Ti samples to consider both open and closed pores contained in the samples. Open pores are the well-defined pores intentionally introduced by the present structural design, whereas closed pores are a smaller-scale by-product of the manufacturing process. Therefore it is necessary to distinguish between these types of pores in the samples to understand the properties of porous Ti listed below.

(i) Apparent density

The apparent density was obtained using Archimedes' principle, which can provide the density with a very high accuracy and repeatability. The apparent density ρ_{apparent} of a sample can be described as

$$\rho_{\text{apparent}} = \frac{m_{\text{air}}}{m_{\text{air}} - m_{\text{water}}} \rho_{\text{water}},$$

where m_{air} is the mass of the sample in air, m_{water} is its mass in water, and ρ_{water} is temperature-corrected density of distilled water. The masses of the samples were measured using an analytical balance (AUW120D, Shimadzu, Japan). The samples were dried at 383 K for 30 min under vacuum before the measurement, and the distilled water was heated to 353 K for 1 h to remove any dissolved gas. This density represents the solid part; that is, the volume of the closed pores is included, whereas that of the open ones is excluded.

(ii) Bulk density

The bulk density was obtained from the apparent volume of the sample and its mass in air. The bulk density ρ_{bulk} is defined as

$$\rho_{\text{bulk}} = \frac{m_{\text{air}}}{L^2 \times H}.$$

The apparent length L and height H of the porous samples were measured using a digital micrometre.

(iii) Filling fraction

The filling fraction of Ti in a porous sample can then be calculated from the two densities as

$$\text{Filling fraction} = \frac{\rho_{\text{bulk}}}{\rho_{\text{apparent}}}.$$

(iv) Porosity

In addition, the volume fraction of open pores, or porosity, is defined as the ratio of open space to the apparent bulk volume. Thus, the porosity can be obtained from the filling fraction as

$$\text{Porosity [\%]} = (1 - \text{Filling fraction}) \times 100.$$

2.3 Compressive test

The fabricated prismatic samples were used in a mechanical test. A compression test was conducted at an initial strain rate of $1.74 \times 10^{-3}\,s^{-1}$ for the porous Ti samples using a tensile tester (Autograph AG-X Plus, Shimadzu, Japan) with a 5 kN load cell. A mechanical test using a strain gauge is necessary to determine Young' modulus of samples. However it could not be applied to the present porous samples. In the present study, the strain was obtained from the stroke displacement and the gradient of the stress-strain curve in elastic region was defined as α instead of the Young's modulus. Then the ratio of the gradient in porous Ti α to that in the dense sample α_1 was obtained for each porous Ti in order to compare the parameter related to Young's modulus. The 0.2% proof stress of the samples were also determined from the stress–strain curves.

3. Results and Discussion

3.1 Characterisation of porous titanium

Five types of porous Ti samples and one dense Ti sample were fabricated with the laser AM machine (EOSINT M 270, EOS, Germany). The appearances of the samples were observed using a digital camera (Stylus TG-4 Tough, Olympus) and are shown in Fig. 2. The fabricated porous structures appear as designed, though the flat planes in the rhombicuboctahedron-derived unit structure could not be precisely reproduced as a result of surface tension during melting. In addition, the region where the connection faces of the unit structures are joined (connection regions) have a cylindrical shape in the porous Ti samples with $w/l = 0.30$ and 0.35. No significant visible distortion was observed in any of the samples on the whole.

The connection regions in the longitudinal direction were also observed by scanning electron microscopy (SEM) (Fig. 3). The shape of the powders remained on the surface in all samples. The shape of the connection region did not accurately reproduce that in the CAD design in some cases. For the specimens with $w/l = 0.30$ and 0.35, the neck of the connection region was again confirmed to show a cylindrical shape by SEM observation, as in the digital camera observation. Interestingly, the powders were completely melted in the connection regions. This may have been due to a heterogeneous heat flow induced by the structure. The heat flow from the thick parts seemed to be hindered by the thin necks. Clearance was clearly observed around the connection regions of the unit structures even in the case of $w/l = 0.95$. This means that a structural design that takes into account the heat flow and solid-

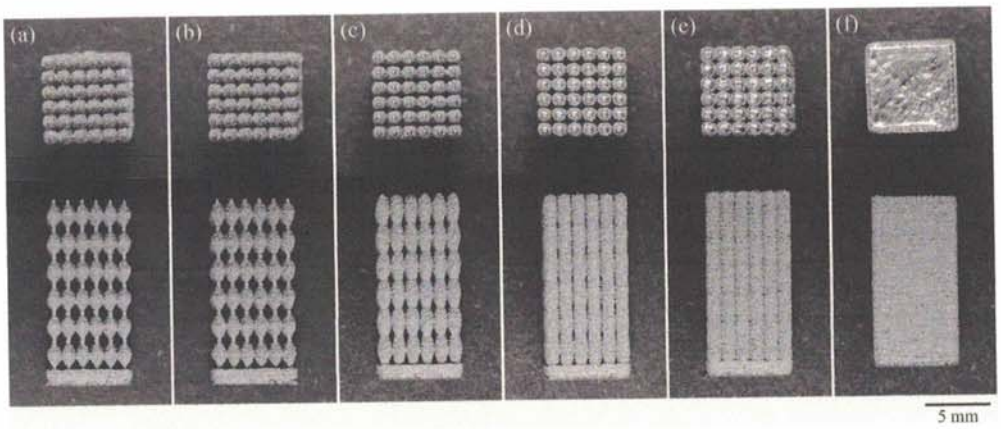

Fig. 2 Top and side views of porous Ti samples prepared by the laser additive manufacturing with $w/l =$ (a) 0.30, (b) 0.35, (c) 0.60, (d) 0.80, (e) 0.95, and (f) dense.

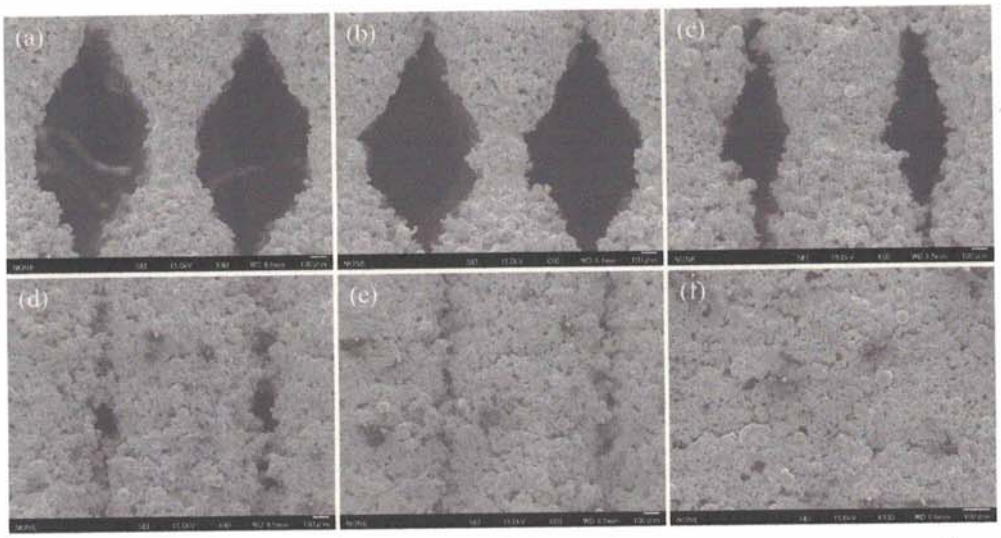

Fig. 3 SEM images of the neck of a connection region in the loading direction in additively manufactured porous Ti samples with $w/l =$ (a) 0.30, (b) 0.35, (c) 0.60, (d) 0.80, (e) 0.95, and (f) dense.

ification speed is necessary to accurately reproduce the designed shape.

The porous specimens were imaged by micro-computed tomography (μCT) (inspeXio SMX-90CT Plus, Shimadzu, Japan) at a tube current of 110 μA, a tube voltage of 90 kV, a scan time of 20 min, and a resolution of 10 μm with a total 272 projections. To quantitatively analyse the structure, image analysis was carried out using ImageJ, a public domain Java-based image processing program developed by the National Institute of Health.[20,21]

Figure 4(a) and (b) shows the μCT images sliced perpendicular to the load axis along the height direction at the levels of maximal and minimal cross-sectional area, respectively, in the porous Ti sample with $w/l = 0.30$ as an illustrative example. The images correspond to planes passing through the centre and connecting face, respectively, of a rhombicuboctahedron-derived unit. The solid Ti parts can be clearly recognised with this technique. No printing failure regions were confirmed in any of the additively manufactured porous Ti samples. Therefore, it can be said that the present process parameters were optimised for the fabrication of the present porous structure in pure Ti. In addition, all pores were confirmed to be connected even in the porous structure with $w/l = 0.95$ by the μCT analysis. Porous titanium with diamond unit structure was reported to show significantly higher fixation ability in the pore size of

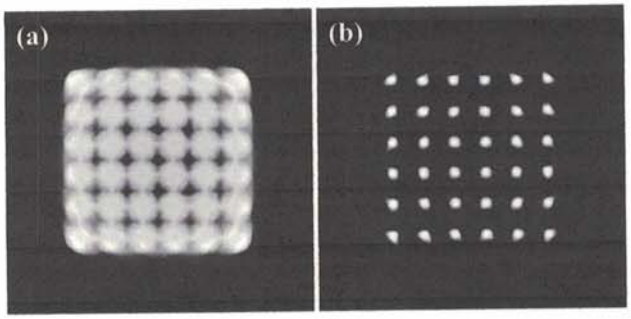

Fig. 4 X-ray μCT images of the porous Ti sample with $w/l = 0.30$. Images were sliced perpendicular to the load axis in the planes of (a) maximal and (b) minimal cross-sectional area.

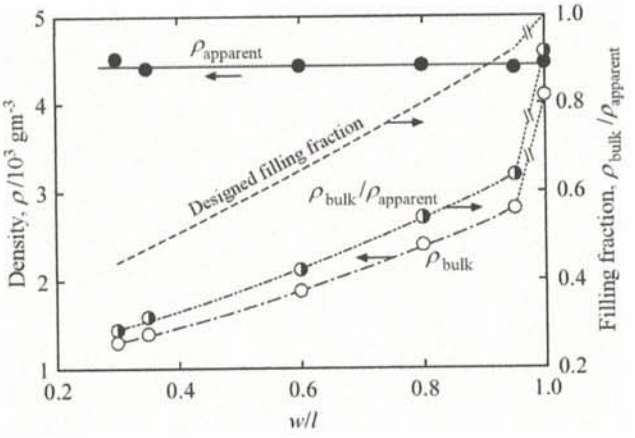

Fig. 5 Apparent and bulk densities of porous Ti samples and filling fraction of Ti in the porous structures.

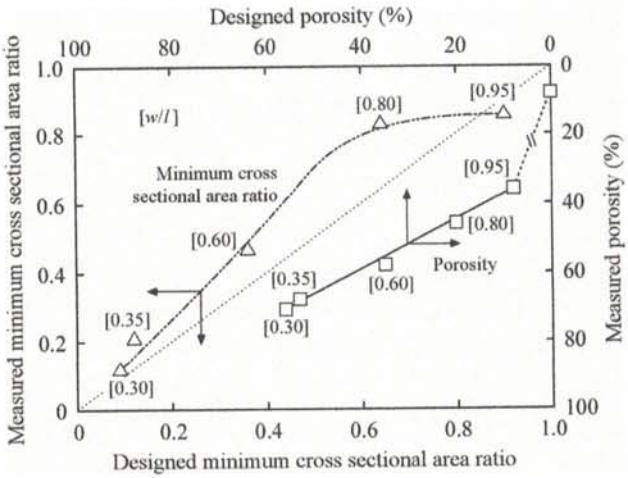

Fig. 6 Designed and measured values of the minimum cross-sectional area ratio and porosity in porous Ti structures.

600 μm.[22] The pore size should be optimised in the end products.

Two types of densities, the apparent and bulk densities, were measured to evaluate the volumes of open and closed pores in the porous Ti samples. As stated previously, open pores are spaces introduced intentionally by the structural design, whereas closed pores are voids in the solid portion of pure Ti introduced as a by-product of the manufacturing process. The two densities are plotted against w/l in Fig. 5. The apparent density was measured by Archimedes' principle. No obvious differences among the densities of the structures were conformed. The average value was calculated to be approximately $4.44 \times 10^3\,\mathrm{gm}^{-3}$, which is a reasonable value. Furthermore, the solid part can be characterised as dense with few solidification voids because the density of a pure Ti plate (ASTM grade 1, thickness of 1 mm, The Nilaco Corporation) was measured to be $4.41 \times 10^3\,\mathrm{gm}^{-3}$ by the same measurement technique.

In contrast, the bulk density increased smoothly with increasing w/l. From the densities, the filling fraction of the solid Ti in the porous structures was calculated, as shown in Fig. 5. Because the apparent density was almost constant with w/l, the filling fraction of Ti showed the same tendency as the bulk density, which increased with increasing w/l. The measured Ti filling fraction of each sample was lower than the design filling fraction for all considered values of w/l. There were relatively large gaps between the bulk density and filling fraction of the sample with $w/l = 0.95$ and those of the dense sample. However, this is not surprising; even as w/l approaches 1, the porous structure does not approach a dense solid, because the value of t was fixed at 0.3 mm.

The designed and measured values of the minimum cross-sectional area ratio and porosity were compared, as shown in Fig. 6. The measured area ratio at the neck of the connection region, i.e. the minimum area ratio, was larger than the designed area ratio for all samples except for that with $w/l = 0.95$. The difference between the measured and designed area ratios increased with increasing w/l up to 0.80 and then saturated. Basically, the minimum area ratio showed that the actual solid region tended to be slightly larger than the designed one because of the region heated by the laser and the related thermal conduction. In the region of small w/l, however, the effect of solidification shrinkage may strongly affect the cross-sectional area ratio. As a result, the difference between the measured and the designed area ratios was small. From the above minimum area ratio results, it was expected that the measured porosity would be smaller than the designed porosity; however, the measured porosity was clearly larger than that in the design. These results indicate that substantial solidification shrinkage occurs around the thick part of each rhombicuboctahedron-derived unit, i.e. at the barrel portion of the unit. In addition, all angular corners in the unit structure became rounded during fabrication because of the surface tension of the powder in the liquid state. The resulting volume reduction also contributed significantly to the higher measured porosity.

Although there were observable differences between the measured and designed values of the cross-sectional area ratio and porosity, they were very small. The measured and designed porosity showed a good linear relationship. It should be noted that the porous Ti structure as a whole can be fabricated as designed despite having a fine structures on the sub-millimetre scale.

3.2 Mechanical properties

A compressive test was performed to compare the mechanical properties of the structures with different unit dimensions. Figure 7 shows the stress–strain curves of the additively manufactured porous Ti samples. All stress–strain curves were typical and smooth, as in ductile bulk metals. The gradients of the curves in elastic region and the proof stresses were obtained from the stress–strain curves. In the sample with $w/l = 0.30$ and 0.35, loading was stopped after yielding was confirmed. In the other samples, loading was applied to the limitation of the equipment, 5 kN. As a result, yielding could not be confirmed in the samples with $w/l =$ 0.80 and 0.95 or the dense sample.

Figure 8 shows 3D CT images of the porous Ti sample with $w/l = 0.30$ deformed to a plastic strain of 1.9%. As shown in these images, the necks of the connection regions at the centre of the sample in the height direction buckled. Because such buckling or bending was not visually observed during elastic deformation, it can be concluded that the

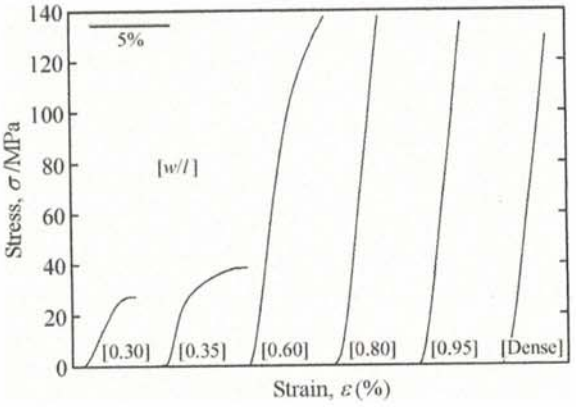

Fig. 7 Stress–strain curves in additively manufactured porous Ti samples.

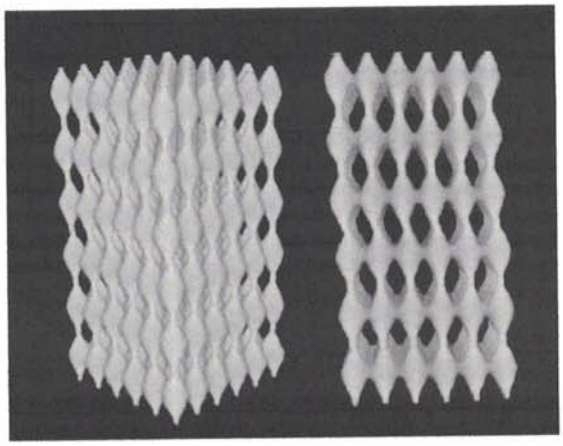

Fig. 8 3D image of the porous Ti sample with $w/l = 0.30$ after compressive deformation up to $\varepsilon = 1.9\%$.

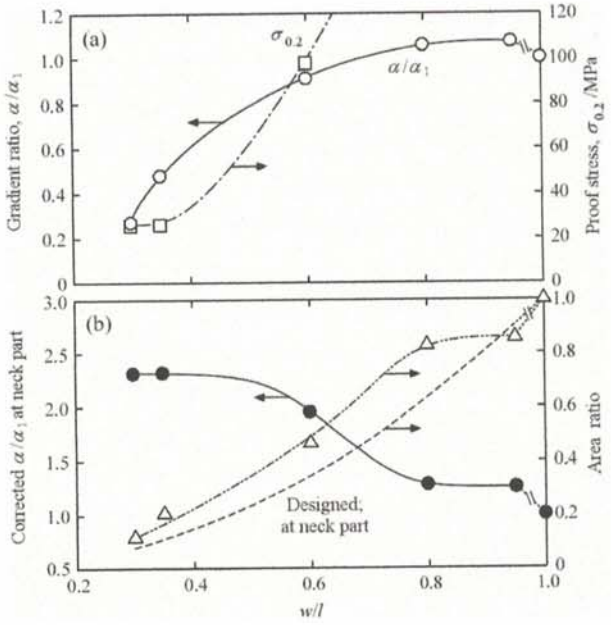

Fig. 9 (a) Ratio of the gradient of porous Ti α to that of dense sample α_1 and 0.2% proof stress $\sigma_{0.2}$ in porous Ti with different w/l values and dense samples. (b) Ratio of the minimum cross-sectional area to the nominal cross-sectional area of porous Ti samples in the plane perpendicular to the load axis measured by using μCT, and corrected gradient ratio at neck part calculated from the gradient ratio α/α_1 and the measured minimum cross-sectional area ratio.

yielding observed in the stress–strain curves is due to this buckling.

The gradient ratios α/α_1 and proof stresses $\sigma_{0.2}$ obtained from the stress–strain curves for the porous Ti samples are plotted against w/l in Fig. 9(a). The gradient ratio increased with increasing w/l, saturated above $w/l = 0.8$, and decreased slightly in the dense sample prepared as a rectangular parallelepiped. The yield stress increased drastically with increasing w/l. The yield stress could not be measured in the porous Ti samples with $w/l = 0.8$ and 0.95 and the dense sample because of the limitations of the equipment.

Up to now, mechanical properties in porous materials were discussed mainly from the viewpoint of porosity.[23–25] Actually, the present mechanical property depending on the structure can be explained from it as well. In the present study, however, we discussed the structural dependence of mechanical property in detail.

In the present compressive test, the regions surrounding the locations of minimal cross-sectional area in the plane perpendicular to the loading axis bore the entire load. Actually, it can be seen from the 3D images of the porous Ti sample after deformation (Fig. 8) that the necks of the connection regions experienced high loading.

The ratio of the minimum cross-sectional area to the nominal cross sectional area of the porous Ti samples in the plane perpendicular to the load axis and the corrected gradient ratio calculated from this area ratio are also plotted against w/l in Fig. 9(b). The corresponding designed area ratio is also plotted as a broken line. The measured area ratios were slightly larger than the designed area ratios, but both showed the same trend, as mentioned above. The corrected gradient ratio was then re-calculated under the assumption that the load was borne exclusively by the regions of minimal cross-sectional area (Fig. 9(b)). In the porous Ti samples with $w/l \geq 0.80$, the corrected gradient ratio was approximately 1.2, which is almost equivalent to that in the dense Ti. In contrast, in the samples with greater porosity, the corrected gradient ratio was larger, reaching approximately 2.3 at $w/l = 0.30$ and 0.35. The value was almost twice that of the dense one in spite of similar solidified titanium in both samples. This indicates that the neck parts with small w/l may have solidified after completely melting. In the portion except for the necks, it implies that the local Young's modulus in the AM samples did not reach that of melted pure Ti ingot. Furthermore, the microstructure including a texture might be important to understand this phenomenon clearly. Further experiments would be required in order to clarify the effect of microstructure on the mechanical properties in the AM titanium.

Thus, the mechanical properties such as Young's modulus and proof stress of porous Ti can be arbitrarily controlled by changing the area ratio at the connection regions of the units in the plane perpendicular to the loading axis. However, it should be noted that the local mechanical properties depending on the portions of the samples are not uniform. The present proposed structure is excellent in that the mechanical properties can be easily controlled while

maintaining the connectivity of all of the pores. In addition, other structural parameters such as t/h can be independently changed. According to the present porous structure, the anisotropy of the mechanical properties can also be easily controlled by changing the aspect ratio of the rhombicuboctahedron-derived units. Comprehensive understanding of the effects of structural and process parameters on microstructure including texture and mechanical property is required to produce high performance and functionality porous materials.

4. Summary

Porous Ti samples composed of rhombicuboctahedron-derived units with sub-millimetre dimensions were fabricated by laser additive manufacturing. The dependence of the mechanical properties of the fabricated samples on the structural parameters was also investigated. The following conclusions can be drawn from this study.

(1) Porous Ti structures composed of rhombicuboctahedron-derived units can be accurately fabricated as designed by laser additive manufacturing even when the units have sub-millimetre dimensions.

(2) The apparent densities of the solid portion of the porous Ti structures were almost equal for all samples at approximately $4.44 \times 10^3\,\mathrm{gm}^{-3}$. No remarkable solidification voids were introduced in the fabrication process. The porosity can be easily controlled with the present structural design; the measured and designed porosities showed a good linear relationship, though the measured porosity was slightly larger than the designed porosity. This may have been the result of remarkable solidification shrinkage at the thick part of the rhombicuboctahedron-derived units.

(3) The gradient of stress-strain curve in elastic region increases as the minimum cross-sectional area ratio in the plane perpendicular to the loading axis increases. This indicates the Young's modulus of porous Ti can be arbitrarily controlled by adjusting the design parameters of the present structure. However, it should be noted that the local mechanical properties such as Young's modulus depending on the portions are not uniform.

Acknowledgement

The authors would like to thank Chang Tinghsuan, Yohei Fujimoto and Maria Adachi for their assistance with the image analysis and the mechanical testing. This work was supported in part by the Light Metal Educational Foundation, Inc.

REFERENCES

1) N. Sumitomo, K. Noritake, T. Hattori, K. Morikawa, S. Niwa, K. Sato and M. Niinomi: J. Mater. Sci. Mater. Med. **19** (2008) 1581–1586.
2) M. Niinomi, M. Nakai and J. Hieda: Acta Biomater. **8** (2012) 3888–3903.
3) T. Ahmed, M. Long, J. Silvestri, C. Ruiz and H.J. Rack: *Titanium '95: Science and Technology*, ed. by P.A. Blenkinsop, W.J. Evans and H.M. Flower, (The Institute for Materials, Birmingham, UK, 1996) pp. 1760–1767.
4) D. Kuroda, M. Niinomi, M. Morinaga, Y. Kato and T. Yashiro: Mater. Sci. Eng. A **243**(1–2) (1998) 244–249.
5) N. Nomura, T. Kohama, I.H. Oh, S. Hanada, A. Chiba, M. Kanehira and K. Sasaki: Mater. Sci. Eng. C **25** (2005) 330–335.
6) C.E. Wen, M. Mabuchi, Y. Yamada, K. Shimojima, Y. Chino and T. Asahina: Scr. Mater. **45** (2001) 1147–1153.
7) I.K. Oh, N. Nomura and S. Hanada: Mater. Trans. **43** (2002) 443–446.
8) H. Li, S.M. Oppenheimer, S.I. Stupp, D.C. Dunand and L.C. Brinson: Mater. Trans. **45** (2004) 1124–1131.
9) M. Takemoto, S. Fujibayashi, M. Neo, J. Suzuki, T. Kokubo and T. Nakamura: Biomaterials **26** (2005) 6014–6023.
10) I.-H. Oh, N. Nomura, N. Masahashi and S. Hanada: Scr. Mater. **49** (2003) 1197–1202.
11) M. Ueda, N. Hayashi, Y. Nakano, M. Ikeda, K. Doi, S. Mori, H. Kitagaki, S. Terauchi and A. Seki: Mater. Trans. **57** (2016) 2002–2007.
12) T. Nakano, K. Kaibara, Y. Tabata, N. Nagata, S. Enomoto, E. Marukawa and Y. Umakoshi: Bone **31** (2002) 479–487.
13) T. Ishimoto, T. Nakano, Y. Umakoshi, M. Yamamoto and Y. Tabata: J. Bone Miner. Res. **28** (2013) 1170–1179.
14) B. Levine: Adv. Eng. Mater. **10** (2008) 788–792.
15) G. Lewis: J. Mater. Sci. Mater. Med. **24** (2013) 2293–2325.
16) R. Hedayati, S.A. Yavari and A.A. Zadpoor: Mater. Sci. Eng. C **76** (2017) 457–463.
17) S. Amin Yavari, J. van der Stok, Y.C. Chai, R. Wauthle, Z.T. Birgani, P. Habibovic, M. Mulier, J. Schrooten, H. Weinans and A.A. Zadpoor: Biomaterials **35** (2014) 6172–6181.
18) A.L. Jardini, M.A. Larosa, C.A. de Cavalho Zavaglia, L.F. Bernardes, C.S. Lambert, P. Kharmandayan, D. Calderoni and R.M. Filho: Virtual Phys. Prototyp. **9** (2014) 115–125.
19) C. Mertens, H. Lowenheim and J. Hoffmann: J. Cranio. Maxill. Surg. **41** (2013) 219–225.
20) W.S. Rasband: ImageJ, U. S. National Institutes of Health, Bethesda, Maryland, USA, http://imagej.nih.gov/ij/, (1997–2012).
21) C.A. Schneider, W.S. Rasband and K.W. Eliceiri: Nat. Methods **9** (2012) 671–675.
22) N. Taniguchi, S. Fujibayashi, M. Takemoto, K. Sasaki, B. Otsuki, T. Nakamura, T. Matsushita, T. Kokubo and S. Matsuda: Mater. Sci. Eng. C **59** (2016) 690–701.
23) N. Sudarmadji, J.Y. Tan, K.F. Leong, C.K. Chua and Y.T. Loh: Acta Biomater. **7** (2011) 530–537.
24) S.Y. Chen, C.N. Kuo, Y.L. Su, J.C. Huang, Y.C. Wu, Y.H. Lin, Y.C. Chung and C.H. Ng: Mater. Charact. **138** (2018) 255–262.
25) L.E. Murr: J. Mech. Behav. Biomed. Mater. **76** (2017) 164–177.